Research Article | Vol. 34, No. 22 / 2 Nov 2026 / Optics Express 42188

Optics EXPRESS

Coherent phase manipulation of photonic spin Hall shifts in double-tripod configurations

YONG-HONG MA,[1] MUQADAR ABBAS,[2] JULIUS RUSECKAS,[3] AND HAMID R. HAMEDI[4,*]

[1]School of Science, Inner Mongolia University of Science and Technology, Baotou 014010, China
[2]School of Science, Shenyang Urban Construction University, Shenyang 110167, China
[3]Baltic Institute of Advanced Technology, LT- 01403 Vilnius, Lithuania
[4]Institute of Theoretical Physics and Astronomy, Vilnius University, Sauletekio 3, Vilnius 10257, Lithuania
[*]hamid.hamedi@tfai.vu.lt

Abstract: We theoretically investigate the transverse photonic spin Hall effect (PSHE) in a cavity structure containing a double-tripod (DT) atomic medium. We show that the internal topology of the double-tripod system can be coherently reconfigured through the relative phase of the control fields and the two-photon detuning, leading to qualitatively distinct effective configurations. These structural transformations reshape the transparency bandwidth, absorption spectrum, and dispersive slope, which in turn govern the spin-dependent reflection phase responsible for the PSHE. We demonstrate that large transverse shifts emerge in low-loss dispersive windows and are strongly enhanced near the Brewster angle due to the sensitive dependence of the reflection phase on the optical response. The magnitude, spectral range, and even sign of the spin-dependent displacement can be reversibly tuned by adjusting the phase, detuning, and atomic density. Our results reveal that cavity-assisted DT media provide a reconfigurable platform in which internal quantum interference directly maps to controllable spin–orbit photonic transport.

© 2026 Optica Publishing Group under the terms of the Optica Open Access Publishing Agreement

1. Introduction

Coherent optical driving of atomic media enables a broad class of quantum-optical effects in which long-lived atomic coherences strongly reshape absorption, dispersion, and light-transport characteristics [1–4]. A central illustration is electromagnetically induced transparency (EIT), where destructive quantum interference between excitation pathways eliminates resonant absorption and opens a narrow transparency window accompanied by steep normal dispersion [5–7]. These coherence-engineered dispersive features underpin slow-light phenomena, allowing substantial suppression of probe group velocity and facilitating reversible conversion between propagating optical fields and collective atomic excitations [8–12].

EIT-enabled slow light has been widely explored in three- and four-level media, notably in Λ-type and tripod schemes, where multiple coupling channels provide versatile control of polaritonic evolution and nonlinear optical behavior [8,9]. To access more intricate interference mechanisms and increased parameter control, EIT has been extended to higher-dimensional multilevel configurations [13–16]. In this context, the five-level double-tripod (DT) system is especially appealing because it allows precise coherence tailoring and offers a flexible route to advanced slow light effects, including spinor slow light with an intrinsic two-component degree of freedom [17,18]. A recent work has demonstrated a phase-controllable mechanism for generating optical torque in such a five-level DT atom-light coupling scheme [19], emphasizing the unique coherence properties of this system and its potential for precise quantum control and manipulation of light-matter interactions.

The photonic spin Hall effect (PSHE) represents another fundamental manifestation of spin–orbit coupling in optics, whereby a light beam experiences a polarization-dependent transverse displacement upon interaction with refractive-index gradients [20]. This effect arises

#604918 https://doi.org/10.1364/OE.604918
Journal © 2026 Received 13 May 2026; revised 24 Aug 2026; accepted 8 Oct 2026; published 27 Oct 2026

Optics EXPRESS

from the coupling between a photon's spin angular momentum (polarization) and its propagation trajectory, providing an optical analogue of the electronic spin Hall effect [21]. In this framework, spatial variations of the dielectric environment act as effective fields that generate opposite lateral shifts for the two circular polarization components [20,22,23]. Theoretical foundations were established by Onoda *et al.* [20], while subsequent work connected PSHE to conservation laws and geometric phases [22]. Experimentally, the observation of PSHE was enabled by weak-measurement techniques that amplify subwavelength beam shifts [24]. Today, PSHE serves as a sensitive probe of spin–orbit physics and underpins applications in precision metrology, quantum photonics, and advanced imaging [21,25–28].

Motivated by these considerations, we investigate the PSHE in a platform utilizing a coherently driven DT atomic medium [19]. In our setup, a TM-polarized probe is reflected off a cavity mirror that surrounds the multilevel medium, where quantum interference induces a narrow, highly tunable dispersive feature. Unlike traditional Λ-type, double-Λ, and tripod configurations, the DT arrangement introduces additional interference pathways, allowing for flexible manipulation of the effective refractive-index profile experienced by the two spin components. As a result, the reflected probe gains a spin-dependent transverse displacement, which can be controlled by optical parameters, providing a reconfigurable approach to spin-selective beam steering and coherence-assisted spin-orbit photonic functionality.

2. Theoretical model: double-tripod medium and susceptibility

We examine a five-level double-tripod (DT) atom-light interaction model consisting of three ground states $|0\rangle$, $|1\rangle$, and $|2\rangle$, as well as two excited states $|A\rangle$ and $|B\rangle$. Two weak probe fields, E_A and E_B, correspond to the transitions $|0\rangle \leftrightarrow |A\rangle$ and $|0\rangle \leftrightarrow |B\rangle$, respectively, with Rabi frequencies Ω_{A0} and Ω_{B0}. Four strong control fields couple the excited states to the other ground states: Ω_{A1} and Ω_{A2} drive transitions $|1\rangle \leftrightarrow |A\rangle$ and $|2\rangle \leftrightarrow |A\rangle$, while Ω_{B1} and Ω_{B2} drive transitions $|1\rangle \leftrightarrow |B\rangle$ and $|2\rangle \leftrightarrow |B\rangle$. These control fields form a closed-loop coherent subsystem within the DT structure, enabling quantum interference and coherent control over the internal dynamics of the atomic ensemble. The decay rate of the excited state is Γ, and a two-photon detuning δ shifts the ground states $|1\rangle$ and $|2\rangle$ by $+\delta$ and $-\delta$, respectively. We operate within the weak-probe (linear response) regime, where the population predominantly resides in the ground state $|0\rangle$.

The Hamiltonian interaction describing the system, under the convention $\hbar = 1$, reads:

$$\begin{aligned} H = &(-\Omega_{A0}|A\rangle\langle 0| - \Omega_{B0}|B\rangle\langle 0| - \Omega_{A1}|A\rangle\langle 1| - \Omega_{A2}|A\rangle\langle 2| \\ &- \Omega_{B1}|B\rangle\langle 1| - \Omega_{B2}|B\rangle\langle 2|) + \text{H.c.} - \delta(|2\rangle\langle 2| - |1\rangle\langle 1|) \end{aligned} \tag{1}$$

To facilitate analysis of system dynamics, for each subsystem we define a bright state (coupled) and a dark state (decoupled) with respect to the levels $|A\rangle$ and $|B\rangle$. For the subsystem interacting with $|A\rangle$, these states are given by:

$$|\mathcal{B}_A\rangle = \frac{\Omega_{A1}^*|1\rangle + \Omega_{A2}^*|2\rangle}{\Omega_A}, \tag{2}$$

$$|\mathcal{D}_A\rangle = \frac{\Omega_{A2}|1\rangle - \Omega_{A1}|2\rangle}{\Omega_A}, \tag{3}$$

where $\Omega_A = \sqrt{\Omega_{A1}^2 + \Omega_{A2}^2}$. The bright and dark superpositions associated with the coupling to $|B\rangle$ are defined as

$$|\mathcal{B}_B\rangle = \frac{\Omega_{B1}^*|1\rangle + \Omega_{B2}^*|2\rangle}{\Omega_B}, \tag{4}$$

Optics EXPRESS

$$|\mathcal{D}_B\rangle = \frac{\Omega_{B2}|1\rangle - \Omega_{B1}|2\rangle}{\Omega_B}, \tag{5}$$

with $\Omega_B = \sqrt{\Omega_{B1}^2 + \Omega_{B2}^2}$. The quantities Ω_A and Ω_B denote the effective Rabi frequencies that couple the states $|A\rangle$ and $|B\rangle$ to their respective bright states.

Rewriting the Hamiltonian in the dressed basis $\{|\mathcal{B}_A\rangle, |\mathcal{D}_A\rangle, |\mathcal{B}_B\rangle, |\mathcal{D}_B\rangle\}$, one obtains a simplified representation given by

$$\begin{aligned} H = &(-\Omega_{A0}|A\rangle\langle 0| - \Omega_{B0}|B\rangle\langle 0| - \Omega_A|A\rangle\langle\mathcal{B}_A| - \Omega_B|B\rangle\langle\mathcal{B}_B|) \\ &+ \text{H.c.} - \delta(C_B|\mathcal{B}_A\rangle\langle\mathcal{B}_A| + C_D|\mathcal{D}_A\rangle\langle\mathcal{D}_A| + C_X|\mathcal{B}_A\rangle\langle\mathcal{D}_A| \\ &+ C_X^*|\mathcal{D}_A\rangle\langle\mathcal{B}_A|). \end{aligned} \tag{6}$$

The coefficients entering the detuning-dependent part are

$$C_B = |\Omega_{A2}|^2 - |\Omega_{A1}|^2, \tag{7}$$

$$C_D = -C_B, \tag{8}$$

$$C_X = -\frac{\Omega_{A1}\Omega_{A2} + \Omega_{A1}^*\Omega_{A2}^*}{|\Omega_{A1}|^2 + |\Omega_{A2}|^2}. \tag{9}$$

The evolution of the probe fields and the associated atomic coherences in the DT scheme is governed by the optical Bloch equations. The relevant slowly varying density-matrix elements are defined as

$$\rho_A \equiv \rho_{A0}, \qquad \rho_B \equiv \rho_{B0}, \qquad \rho_1 \equiv \rho_{10}, \qquad \rho_2 \equiv \rho_{20}. \tag{10}$$

For compactness, we introduce the column vectors

$$\boldsymbol{\rho}_o = \begin{pmatrix} \rho_A \\ \rho_B \end{pmatrix}, \qquad \boldsymbol{\rho}_g = \begin{pmatrix} \rho_1 \\ \rho_2 \end{pmatrix}, \qquad \boldsymbol{\Omega}_0 = \begin{pmatrix} \Omega_{A0} \\ \Omega_{B0} \end{pmatrix}, \tag{11}$$

and further define the control-field coupling matrix, the detuning matrix, and the identity operator as

$$\hat{\Omega} = \begin{pmatrix} \Omega_{A1} & \Omega_{A2} \\ \Omega_{B1} & \Omega_{B2} \end{pmatrix}, \qquad \hat{\delta} = \begin{pmatrix} \delta & 0 \\ 0 & -\delta \end{pmatrix}, \qquad \hat{I} = \begin{pmatrix} 1 & 0 \\ 0 & 1 \end{pmatrix}. \tag{12}$$

Under the weak-probe approximation, where the probe fields are assumed to be much weaker than the control fields, so that the atomic population remains predominantly in the ground state—the optical Bloch equations for the DT system can be written in the compact matrix form

$$\frac{\partial}{\partial t}\boldsymbol{\rho}_o = i\hat{\Omega}\,\boldsymbol{\rho}_g + \left(i\Delta - \frac{\Gamma}{2}\right)\boldsymbol{\rho}_o + i\boldsymbol{\Omega}_0, \tag{13}$$

$$\frac{\partial}{\partial t}\boldsymbol{\rho}_g = i\hat{\Omega}^\dagger\boldsymbol{\rho}_o + i\left(\Delta\hat{I} + \hat{\delta}\right)\boldsymbol{\rho}_g. \tag{14}$$

In the steady-state regime, the time derivatives in Eqs. (13),(14) vanish. From Eq. (14) one gets

$$\boldsymbol{\rho}_g = -\left(\Delta\hat{I} + \hat{\delta}\right)^{-1}\hat{\Omega}^\dagger\boldsymbol{\rho}_o. \tag{15}$$

Substituting Eq. (15) into Eq. (13) and rearranging the resulting expression, we obtain the steady-state solution for the optical coherences:

$$\boldsymbol{\rho}_o = \left[\hat{\Omega}\left(\Delta\hat{I} + \hat{\delta}\right)^{-1}\hat{\Omega}^\dagger - \left(\Delta + \frac{i\Gamma}{2}\right)\hat{I}\right]^{-1}\boldsymbol{\Omega}_0. \tag{16}$$

Optics EXPRESS

Note that we have assumed that all four control fields have identical amplitudes Ω while their phases may differ. Accordingly, the Rabi frequencies are parameterized as

$$\Omega_j = \Omega\, e^{i\phi_j}, \qquad j \in \{A1, A2, B1, B2\}, \tag{17}$$

where ϕ_j is the phase of each field. We define two independent phase combinations:

$$\theta = \phi_{A2} - \phi_{B2}, \qquad \phi = (\phi_{A1} - \phi_{B1}) - \theta, \tag{18}$$

where ϕ represents the total relative phase among all four control fields, and θ provides an additional phase degree of freedom that can be used to control the system's optical response.

In terms of the relevant phases and using the shorthand vectors $\boldsymbol{\rho}_0$ and $\boldsymbol{\Omega}_0$, the steady state optical coherence vector can be expressed as

$$\boldsymbol{\rho}_0 = \mathbf{M}\,\boldsymbol{\Omega}_0, \tag{19}$$

where the matrix $\mathbf{M}$ encodes the linear response of the medium to the probe fields and is explicitly given by

$$\mathbf{M} = \frac{\Delta^2 - \delta^2}{2\Omega^2\Delta^2}\frac{1}{D}\begin{pmatrix} M_{11} & M_{12} \\ M_{21} & M_{22} \end{pmatrix}, \tag{20}$$

with the matrix elements

$$M_{11} = M_{22} = \Delta - \frac{(\Delta^2 - \delta^2)(2\Delta + i\Gamma)}{4\Omega^2}, \tag{21}$$

$$M_{12} = -\Delta\, e^{i(\theta+\phi/2)}\left(\cos\frac{\phi}{2} - i\frac{\delta}{\Delta}\sin\frac{\phi}{2}\right), \tag{22}$$

$$M_{21} = -\Delta\, e^{-i(\theta+\phi/2)}\left(\cos\frac{\phi}{2} + i\frac{\delta}{\Delta}\sin\frac{\phi}{2}\right), \tag{23}$$

and

$$D = \left(1 - \frac{(\Delta^2 - \delta^2)(2\Delta + i\Gamma)}{4\Omega^2\Delta}\right)^2 - \cos^2\frac{\phi}{2} - \frac{\delta^2}{\Delta^2}\sin^2\frac{\phi}{2}. \tag{24}$$

Equation (19) gives ρ_A and ρ_B in a form that can be directly used to compute the probe susceptibilities.

2.1. Susceptibility in terms of ρ_A and ρ_B

In the DT system, each probe channel is affected not only by its direct transition but also by cross-couplings to the other channel. Accordingly, there are four linear susceptibilities to describe the system:

$$\chi_{A1}(\omega_p) = \frac{\mathcal{N}\,|\mathbf{d}_{A0}|^2}{\epsilon_0\hbar}\frac{\rho_A}{\Omega_{A0}}, \quad \chi_{B1}(\omega_p) = \frac{\mathcal{N}\,|\mathbf{d}_{B0}|^2}{\epsilon_0\hbar}\frac{\rho_B}{\Omega_{B0}}, \tag{25}$$

$$\chi_{A2}(\omega_p) = \frac{\mathcal{N}\,\mathbf{d}_{A0}\mathbf{d}^*_{B0}}{\epsilon_0\hbar}\frac{\rho_A}{\Omega_{B0}}, \quad \chi_{B2}(\omega_p) = \frac{\mathcal{N}\,\mathbf{d}_{B0}\mathbf{d}^*_{A0}}{\epsilon_0\hbar}\frac{\rho_B}{\Omega_{A0}}. \tag{26}$$

The effective susceptibility for each probe channel, which enters the PSHE analysis, is obtained by summing the direct and cross contributions:

$$\chi_A(\omega_p) = \chi_{A1}(\omega_p) + \chi_{A2}(\omega_p), \tag{27}$$

$$\chi_B(\omega_p) = \chi_{B1}(\omega_p) + \chi_{B2}(\omega_p). \tag{28}$$

In the special case where $\Omega_{A0} = \Omega_{B0}$ which is the case of our work, the direct and cross susceptibilities for each channel are equal in magnitude, i.e., $\chi_{A1} \simeq \chi_{A2}$ and $\chi_{B1} \simeq \chi_{B2}$.

Optics EXPRESS

These susceptibilities determine the effective permittivity of the DT medium:

$$\epsilon_2 = 1 + \chi_j(\omega_p), \quad j = A, B, \tag{29}$$

where j labels the probe channel coupled to the corresponding DT transition. In the following sections and simulations, we focus on the PSHE for the probe beam Ω_{A0}, using $\chi_A(\omega_p)$. The same methodology can be applied straightforwardly to the $j = B$ channel if desired.

In deriving the susceptibilities above, the steady-state solution is obtained for local values of the probe fields, assuming that the atomic system reaches equilibrium at each point in the medium. In general, however, the probe-field amplitudes depend on the propagation coordinate. In a DT system, the two probe channels are coherently coupled, so that energy can be transferred between the fields with Rabi frequencies Ω_{A0} and Ω_{B0} during propagation. Yet, in the present work, we assume that the distance between the cavity mirrors M_1 and M_2 is sufficiently small such that the redistribution of energy between the two probe channels remains negligible. Under this condition, the susceptibilities can be consistently evaluated using the input probe amplitudes without accounting for their mutual conversion. A quantitative criterion for this regime, as well as conditions under which the inter-channel coupling vanishes, are provided in Appendix A.

3. Theoretical model and calculation of photonic spin Hall effect

We consider the probe light beam Ω_{A0} comprising both TE- and TM-polarization components, incident from vacuum onto the cavity mirror M_1 at an angle θ_{in}, as illustrated in Fig. 1(a). The spatial shift induced by PSHE is then calculated using the susceptibility $\chi_A(\omega_p)$, corresponding to the probe channel coupled to the relevant double-tripod transition.

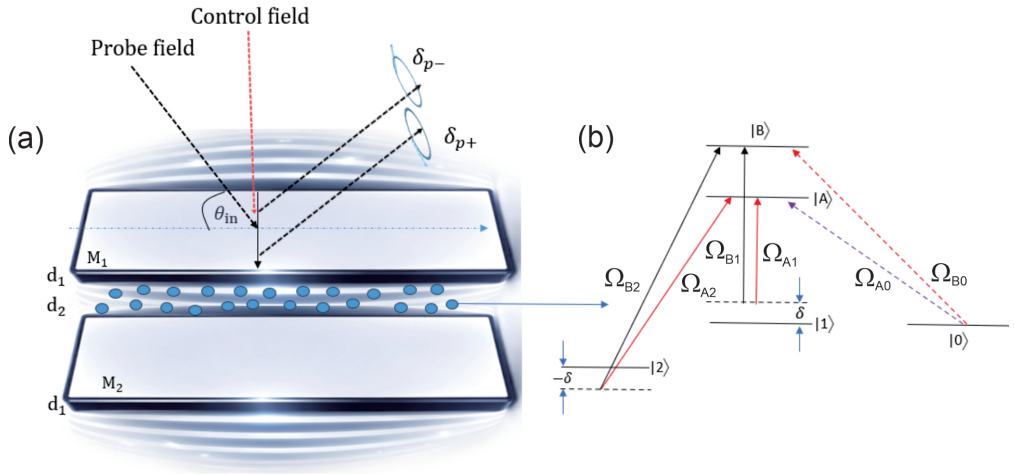


Fig. 1. **(a)** Schematic of a three-layer cavity comprising two mirrors, M_1 and M_2, with a double-tripod (DT) atomic medium placed between them. When a TM-polarized probe beam of Rabi-frequency Ω_{A0} is incident on M_1, the reflected field experiences a spin-dependent spatial splitting. **(b)** Double-tripod level scheme, in which three ground states $|0\rangle$, $|1\rangle$, and $|2\rangle$ are coupled to two excited states $|A\rangle$ and $|B\rangle$. The system is driven by two probe fields Ω_{A0} and Ω_{B0}, along with four strong control fields Ω_{A1}, Ω_{B1}, Ω_{A2}, and Ω_{B2}.

The monochromatic Gaussian probe beam Ω_{A0} can either transmit through or be reflected by the DT atomic system at its interface. Upon reflection, the left- and right-circular polarization components—which are linear combinations of the TE and TM components—separate spatially along the direction orthogonal to the plane of incidence (the y-axis), as depicted in Fig. 1(a). This spin-dependent spatial splitting is referred to as the PSHE.

Optics EXPRESS

The PSHE is a polarization-dependent optical phenomenon that originates from the spin-orbit interaction of light, which causes photons with opposite helicities to deflect in opposite transverse directions. To calculate the PSHE quantitatively, the complex reflection coefficients for the TM-polarized R_M and TE-polarized R_E components of the three-layer structure are obtained using the transfer-matrix approach. These reflection coefficients are given by the following expressions:

$$R_{M,E} = \frac{\mathcal{R}^{12}_{M,E} + \mathcal{R}^{23}_{M,E}\exp(2ik_{2z}q)}{1 + \mathcal{R}^{12}_{M,E}\mathcal{R}^{23}_{M,E}\exp(2ik_{2z}q)}, \tag{30}$$

where q denotes the thickness of the intracavity medium, while $\mathcal{R}^{12}_{M,E}$ and $\mathcal{R}^{23}_{M,E}$ are the reflection coefficients at the mirror 1–medium interface and the medium–mirror 2 interface, respectively.

For a two-layer structure (top mirror–medium–bottom mirror), the reflection coefficient for the TM-polarized component is given by

$$\mathcal{R}^{ij}_{M} = \frac{\epsilon_j k_{iz} - \epsilon_i k_{jz}}{\epsilon_j k_{iz} + \epsilon_i k_{jz}}, \tag{31}$$

and for the TE-polarized component:

$$\mathcal{R}^{ij}_{E} = \frac{k_{iz} - k_{jz}}{k_{iz} + k_{jz}}. \tag{32}$$

Here, $k_{iz} = \sqrt{k_0^2\epsilon_i - k_x^2}$ is the wave vector within the respective layer, while $k_x = \sqrt{\epsilon_1}k_0\sin(\theta_{in})$ denotes the wave vector in the x-direction. Additionally, $k_0 = 2\pi/\lambda$, with λ being the wavelength of the incident light.

Equation (30) indicates that the reflection coefficients are determined by the permittivities of the cavity mirrors ϵ_1 and ϵ_3, which are fixed, as well as by the permittivity of the intracavity medium, ϵ_2, corresponding to the tripod atomic system. Unlike the mirrors, ϵ_2 can be dynamically tuned through the atomic susceptibility $\chi_A(\omega_p)$. The connection between the intracavity permittivity and the susceptibility of the DT medium is expressed as

$$\epsilon_2 = 1 + \chi_A(\omega_p), \tag{33}$$

where $\chi_A(\omega_p)$ is the linear susceptibility of the DT atomic system for the probe field Ω_{A0} used in the present analysis.

This tunability allows for dynamic control over the PSHE of light. When a TM-polarized Gaussian beam reflects from the interface, the field amplitudes of the reflected left- and right-circular polarization components are given by

$$\begin{aligned}\mathcal{E}_r^{\pm}(x_r, y_r, z_r) = \frac{\omega_0}{\omega}\exp\left[-\frac{x_r^2 + y_r^2}{\omega}\right]\times \\ \left[R_M - \frac{2ix_r}{k\omega}\frac{\partial R_M}{\partial\theta_{in}} \mp \frac{2y_r\cot(\theta_{in})}{k\omega}\times\right. \\ \left.(R_E + R_M)\right],\end{aligned} \tag{34}$$

where $\omega = \omega_0\left[1 + \left(\frac{2z_r}{k_1\omega_0^2}\right)^2\right]^{1/2}$, with $z_r = \frac{k_1\omega_0^2}{2}$ is the Rayleigh length, and ω_0 is the beam waist. The coordinates (x_r, y_r, z_r) refer to the reflected-beam reference frame, and the superscript $\pm$ denotes the spin states of the circular components. The transverse displacement of the reflected

Optics EXPRESS

beam is defined as

$$\delta_{p\pm} = \frac{\int y|\mathcal{E}_r^{\pm}(x_r, y_r, z_r)|^2 dx_r dy_r}{\int |\mathcal{E}_r^{\pm}(x_r, y_r, z_r)|^2 dx_r dy_r}. \tag{35}$$

From Eq. (34) and Eq. (35), the transverse spin-dependent displacements δ_{p+} and δ_{p-} can be expressed in terms of the reflection coefficients of the three-layer cavity containing the tripod atomic medium [29]:

$$\delta_{p\pm} = \mp \frac{k_1 \omega_0^2 \mathrm{Re}\left[1 + \frac{R_E}{R_M}\right] \cot(\theta_{in})}{k_1^2 \omega_0^2 + \left|\frac{\partial \ln R_E}{\partial \theta_{in}}\right|^2 + \left|(1 + \frac{R_E}{R_M})\cot(\theta_{in})\right|^2}. \tag{36}$$

Here, $\delta_{p\pm}$ represents the transverse shift of the left and right circularly polarized components, with $k_1 = \sqrt{\epsilon_1} k$. In this work, we focus on the transverse shift δ_{p+} of the left-circularly polarized component. Since the two spin components have equal magnitudes but opposite directions, the shift of the right-circularly polarized component can be inferred directly.

4. Results

We examine how the relative phase of the control fields influences the PSHE displacement. First, we focus on the regime where $\delta \neq 0$ and the control fields maintain a phase difference of π, which can be realized by setting $\phi = \pi$ and $\theta = 0$. In this parameter configuration, the Hamiltonian given in Eq. (1) simplifies to the following form (see Ref. [19]):

$$H = (-\Omega_{A0}|A\rangle\langle 0| - \Omega_{B0}|B\rangle\langle 0| - \Omega_A|A\rangle\langle -| - \Omega_B|B\rangle\langle +|) + \mathrm{H.c.} - \delta\left(|+\rangle\langle -| + |-\rangle\langle +|\right), \tag{37}$$

where $|+\rangle = \frac{1}{\sqrt{2}}(|1\rangle + |2\rangle)$, $|-\rangle = \frac{1}{\sqrt{2}}(|1\rangle - |2\rangle)$, and for equal control-field amplitudes, $\Omega_A = \Omega_B = \sqrt{2}\Omega$. This choice of phases reconfigures the double-tripod system into two coupled Λ subsystems [19]. The first Λ subsystem involves the transitions $|0\rangle \leftrightarrow |A\rangle \leftrightarrow |-\rangle$, while the second involves $|0\rangle \leftrightarrow |B\rangle \leftrightarrow |+\rangle$. The term proportional to$\boldsymbol{\delta}$ introduces cross-talk between these two Λ subsystems. Under this specific configuration, Eq. (19) can be further simplified to describe the dynamics of these effectively coupled Λ systems:

$$\begin{aligned}\begin{pmatrix}\rho_A\\ \rho_B\end{pmatrix} = &\frac{8\Omega^2}{\left[4\Omega^2 - (2\Delta + i\Gamma)(\Delta + \delta)\right]\left[4\Omega^2 - (2\Delta + i\Gamma)(\Delta - \delta)\right]}\\ &\times\begin{pmatrix}\Delta - \frac{(\Delta^2 - \delta^2)(2\Delta + i\Gamma)}{4\Omega^2} & -\delta e^{i\theta}\\ -\delta e^{i\theta} & \Delta - \frac{(\Delta^2 - \delta^2)(2\Delta + i\Gamma)}{4\Omega^2}\end{pmatrix}\begin{pmatrix}\Omega_{A0}\\ \Omega_{B0}\end{pmatrix}\end{aligned} \tag{38}$$

The off-diagonal term $-\delta$ establishes a direct link between the two probe channels, A_0 and B_0. This phase-sensitive interaction modifies the system's response and directly shapes the transverse shifts associated with the PSHE.

We now examine the optical response of the double-tripod medium for the situation where δ is of the order of 100 kHz, Γ is on the order of MHz, following [17]. Figure 2 presents the real and imaginary components of the probe susceptibility χ_A as functions of the normalized detuning Δ/Γ. With the two-photon detuning fixed at $\delta = 0.1\Gamma$, a transparency window emerges around $\Delta/\Gamma = 0$. More precisely, the minimum absorption occurs near $\Delta = \delta$, where the imaginary part of the susceptibility vanishes, while the real part shows a normal dispersion profile. However, at $\Delta/\Gamma = 0$, the absorption remains weak and the dispersion retains its normal character; therefore, we use this detuning in the following discussion for simplicity, particularly in estimating the

Optics EXPRESS

characteristic distance given in Appendix A, Eq. (54). At higher detuning, $\Delta/\Gamma = \sqrt{2}$, the system enters an absorptive regime accompanied by anomalous dispersion. In this case, the imaginary component grows in magnitude, and the real part changes slope, signaling a departure from the interference-induced transparency toward conventional absorption.

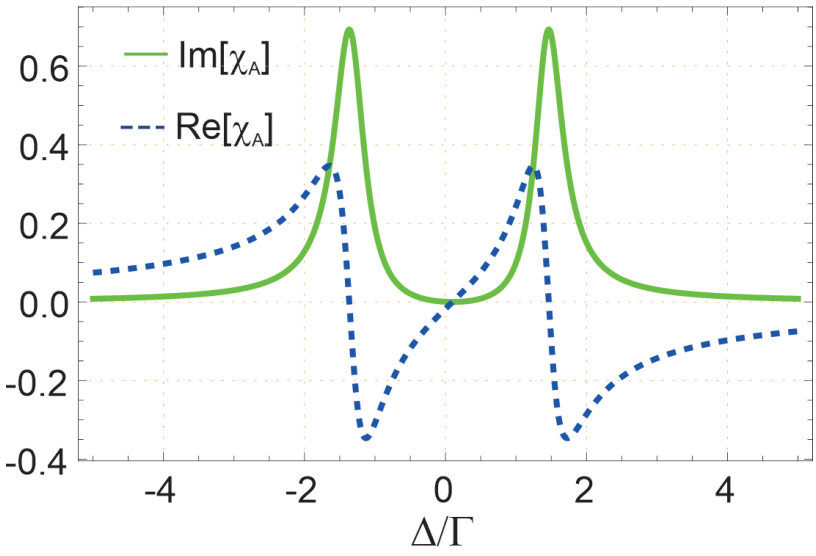


Fig. 2. Real (dashed curve) and imaginary (solid curve) components of the optical susceptibility as functions of the normalized probe detuning Δ/Γ. Unless stated otherwise, the numerical values used are: $\Gamma = 1$ MHz, $\delta = 0.1\Gamma$, $\phi = \pi$, $\theta = 0$, $\Omega = \Gamma$, $\epsilon_0 = 8.85 \times 10^{-12}$ F/m, an atomic number density $\mathcal{N}/V = 10^{12}$ m^{-3}, $\hbar = 1.05 \times 10^{-34}$ J $\cdot$ s, $\mathbf{d}_{A0} = 1.269 \times 10^{-29}$ C m.

The transverse PSHE shift depends on the relative amplitudes of the reflected TE and TM components, R_E and R_M, as defined in Eq. (30). To illustrate this dependence, Fig. 3 displays the ratio $|R_E/R_M|$ as a function of the incidence angle θ_{in} for probe detunings $\Delta/\Gamma = \sqrt{2}$ and $\Delta/\Gamma = 0$ (panels a and c), along with the corresponding PSHE displacements δ_{p+} in panels b and d. These plots show how variations in the reflection coefficients induce spin-dependent transverse shifts.

The ratio $|R_E/R_M|$ exhibits a pronounced peak near the Brewster angle. For $\Delta/\Gamma = \sqrt{2}$ (panel a), the peak is broader, while for $\Delta/\Gamma = 0$ (panel c), the peak is sharper and occurs at its maximum. This enhancement arises because $|R_M|$ approaches zero near the Brewster angle, producing a rapid increase in $|R_E/R_M|$.

The PSHE displacement follows a similar trend: the transverse shift is smaller for $\Delta/\Gamma = \sqrt{2}$ (panel b) and larger for $\Delta/\Gamma = 0$ (panel d) near the Brewster angle. This is due to near-EIT conditions at $\Delta/\Gamma = 0$, where absorption is suppressed and spin-dependent splitting is enhanced. For $\Delta/\Gamma = \sqrt{2}$, residual absorption reduces both the reflection ratio and the corresponding PSHE displacement.

Figure 4 shows the transverse PSHE displacement δ_{p+} as a function of incidence angle θ_{in} and normalized probe detuning Δ/Γ for two atomic densities: (a) $N/V = 10^{12}$ m^{-3} and (b) $N/V = 10^{11}$ m^{-3}. The color map, normalized to the wavelength λ, highlights how the PSHE depends simultaneously on detuning and incidence angle, complementing the trends in Fig. 3. For the higher density (panel a), the maximum transverse shift occurs near $\Delta/\Gamma = 0$ at the Brewster angle $\theta_{\text{in}} \approx 33.5°$, consistent with the EIT condition. At detunings near $\Delta/\Gamma \approx \pm\sqrt{2}$, the displacement decreases significantly. In the lower-density case (panel b), the detuning dependence

Optics EXPRESS

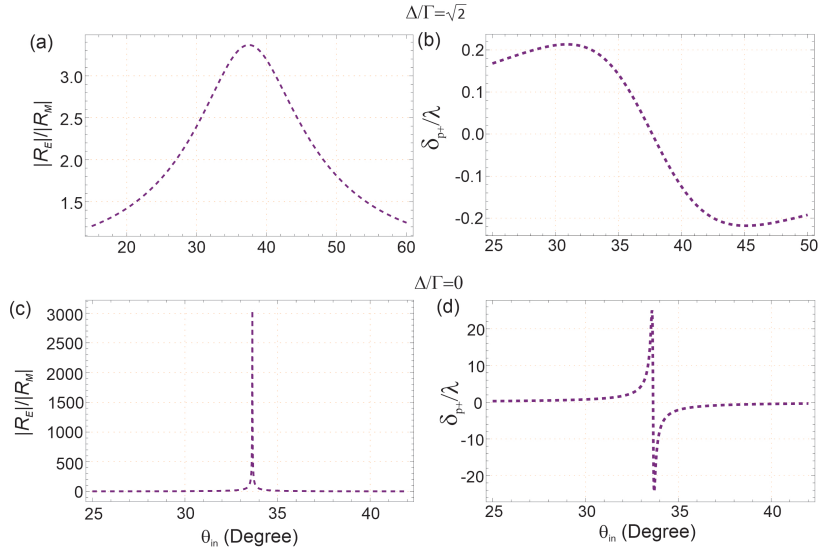


Fig. 3. Dependence of the reflection-coefficient magnitude ratio $|R_E/R_M|$ on the incidence angle θ_{in} for (a) $\Delta/\Gamma = \sqrt{2}$, and (c) $\Delta/\Gamma = 0$. The associated PSHE displacement δ_{p+}/λ as a function of θ_{in} is shown in (b) $\Delta/\Gamma = \sqrt{2}$, and (d) $\Delta/\Gamma = 0$. Unless otherwise stated, the parameters are $\Gamma = 1$ MHz, $\delta = 0.1\Gamma$, $\phi = \pi$, $\theta = 0$, probe-field amplitudes $|\Omega_{A0}| = |\Omega_{B0}| = 0.1\Gamma$, $\Omega = \Gamma$, $\epsilon_0 = 8.85\times10^{-12}$ F/m, $\hbar = 1.05\times10^{-34}$ J · s, atomic density $\mathcal{N}/V = 10^{12}$ m^{-3}, dipole moment $\mathbf{d}_{A0} = 1.269\times10^{-29}$ C m, wavelength $\lambda = 852$ nm, wave number $k_0 = 2\pi/\lambda$, beam waist $\omega_0 = 50\lambda$, $q = 0.1\times10^{-6}$ m, and permittivities $\epsilon_1 = \epsilon_3 = 2.22$, with $\epsilon_2 = 1 + \chi_A(\omega_p)$.

is weaker, showing that reduced atomic density limits the tunability of the PSHE. In both cases, the angular dependence is evident, with the largest shifts near the critical incidence region.

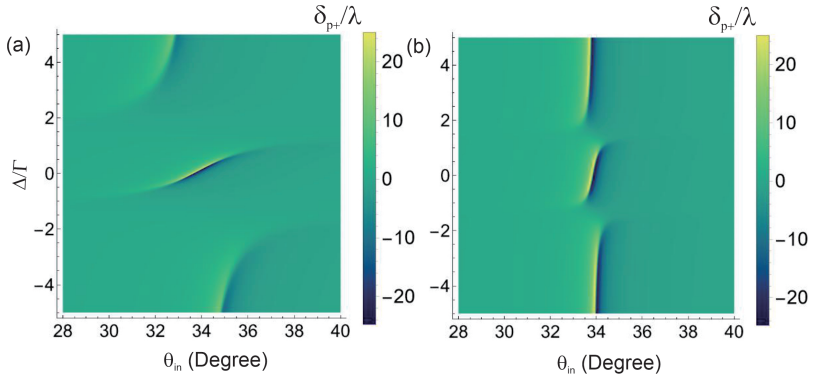


Fig. 4. (a) Transverse photonic spin Hall displacement δ_{p+} plotted against the incidence angle θ_{in} for a density $\mathcal{N}/V = 10^{12}$ m^{-3}. (b) The corresponding δ_{p+}–θ_{in} characteristic when the density is reduced by one decade to $\mathcal{N}/V = 10^{11}$ m^{-3}. The calculations are performed using $\Gamma = 1$ MHz, $\delta = 0.1\Gamma$, $\phi = \pi$, $\theta = 0$, probe-field amplitudes $|\Omega_{A0}| = |\Omega_{B0}| = 0.1\Gamma$, and $\Omega = \Gamma$. Other constants are $\epsilon_0 = 8.85\times10^{-12}$ F/m, $\hbar = 1.05\times10^{-34}$ J · s, $\mathbf{d}_{A0} = \mathbf{d}_{B0} = 1.269\times10^{-29}$ C m, $\lambda = 852$ nm, and $k_0 = 2\pi/\lambda$. The Gaussian beam parameters are $\omega_0 = 50\lambda$ and $q = 0.1\times10^{-6}$ m. The dielectric environment is defined by $\epsilon_1 = \epsilon_3 = 2.22$ and $\epsilon_2 = 1 + \chi_A(\omega_p)$.

Optics EXPRESS

We now examine the scenario in which the relative phases are chosen as $\phi = 0$ and $\theta = 0$, with a two-photon detuning $\delta/\Gamma = 0.1$. In this setting, the Hamiltonian in Eq. (1) takes the form

$$\begin{aligned} H = &-\Omega_A|A\rangle\langle 0| - \Omega_B|B\rangle\langle 0| - \Omega_A|A\rangle\langle +| - \Omega_B|B\rangle\langle +| \\ &+ \text{H.c.} + \delta\left(|+\rangle\langle -| + |-\rangle\langle +|\right). \end{aligned} \tag{39}$$

In this arrangement, the excited states $|A\rangle$ and $|B\rangle$ couple solely to the symmetric superposition $|+\rangle$, forming a double-Λ configuration with two independent Λ-type subsystems: $|0\rangle \leftrightarrow |A\rangle \leftrightarrow |+\rangle$ and $|0\rangle \leftrightarrow |B\rangle \leftrightarrow |+\rangle$. The antisymmetric state $|-\rangle$ remains uncoupled from the excited states directly but interacts with the double-Λ system via the two-photon detuning δ [19]. From Eq. (19), we obtain

$$\begin{aligned} \begin{pmatrix} \rho_A \\ \rho_B \end{pmatrix} = &\frac{-2}{(2\Delta + i\Gamma)\left(2\Delta - \frac{(\Delta^2-\delta^2)(2\Delta+i\Gamma)}{4\Omega^2}\right)} \\ &\times \begin{pmatrix} \Delta - \dfrac{(\Delta^2-\delta^2)(2\Delta+i\Gamma)}{4\Omega^2} & -\Delta e^{i\theta} \\ -\Delta e^{-i\theta} & \Delta - \dfrac{(\Delta^2-\delta^2)(2\Delta+i\Gamma)}{4\Omega^2} \end{pmatrix} \begin{pmatrix} \Omega_{A0} \\ \Omega_{B0} \end{pmatrix} \end{aligned} \tag{40}$$

We analyze the optical response and the associated PSHE shift for this configuration, as illustrated in Fig. 5. Figure 5(a) shows the optical susceptibility χ_A as a function of normalized probe detuning Δ/Γ. The spectrum exhibits a three-peak absorption pattern: the central resonance displays a pronounced narrow absorption peak (high $\text{Im}[\chi_A]$), while the real part shows a steep dispersive slope with rapid sign changes ($\text{Re}[\chi_A]$). In the detuned regions around $\Delta/\Gamma = \pm 0.1$, absorption is strongly suppressed ($\text{Im}[\chi_A] \approx 0$), and the dispersion is normal, creating favorable conditions for enhanced spin-dependent transverse shifts.

Figure 5(b) presents the transverse PSHE displacement δ_{p+}/λ as a function of incidence angle θ_{in} at resonance ($\Delta/\Gamma = 0$). Although the shift depends on angle, its overall magnitude remains relatively small due to residual absorption at resonance, which diminishes the coherent interference required for large spin-dependent displacements. By contrast, Fig. 5(c) shows δ_{p+}/λ for probe detunings $\Delta/\Gamma = \pm 0.2$, where the PSHE reaches its maximum. These detunings lie close to the EIT condition ($\Delta \approx \delta = 0.1\Gamma$), where absorption is minimal ($\text{Im}[\chi_A] \approx 0$), allowing the dispersive phase response to dominate. Consequently, the spin-orbit interaction of the reflected light is enhanced, yielding the largest transverse spin-dependent shifts. Note that for simplicity in the analytical estimation of the characteristic length (Appendix A, Eq. (59)), we adopt $\Delta/\Gamma = \pm 0.2$, and use the same values in the simulations for consistency.

To visualize the combined effect of detuning and incidence angle, Fig. 5(d) provides a colormap of δ_{p+}/λ as a function of both θ_{in} and Δ/Γ. This plot highlights the main observation: the strongest positive and negative transverse shifts occur in low-loss regions where $\text{Im}[\chi_A] \to 0$, while the PSHE is substantially suppressed at the resonant absorption peak ($\Delta/\Gamma = 0$). The map thus clearly demonstrates that maximal spin-dependent displacements are achieved within the transparency windows where dispersive effects dominate over absorption.

Up to this point, the PSHE has been analyzed in the regime of finite two-photon detuning ($\delta \neq 0$). We now turn to the case of vanishing two-photon detuning, $\delta = 0$, and examine how different phase configurations modify the optical response and the associated transverse PSHE shift. Figures 6 and 7 present this comparison for two representative phase settings: ($\phi = \pi, \theta = 0$) and ($\phi = 0, \theta = 0$).

Optics EXPRESS

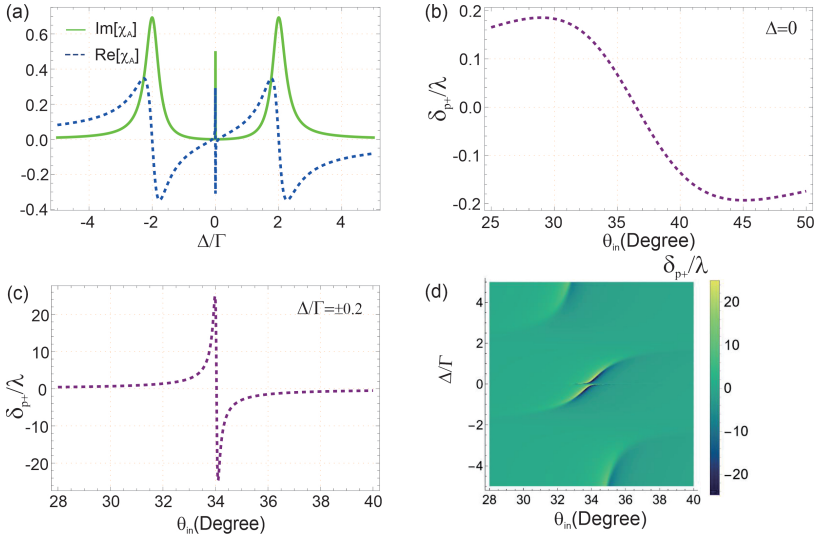


Fig. 5. (a) Optical susceptibility versus the normalized probe detuning Δ/Γ, where the absorptive response is indicated by a solid curve and the dispersive response by a dashed curve. (b) Transverse photonic spin Hall shift δ_{p+} as a function of the incidence angle θ_{in} for resonant probe detuning i.e. $\Delta = 0$. (c) The corresponding δ_{p+}–θ_{in} dependence by considering detuning $\Delta = \pm 0.2\Gamma$. (d) Density plot of PSHE δ_{p+}–θ_{in} as a function of the incidence angle θ_{in} and detuning Δ/Γ. The set of parameters used is: $\Gamma = 1$ MHz, $\phi = 0$, $\theta = 0$, $\delta = 0.1\Gamma$, $|\Omega_{A0}| = |\Omega_{B0}| = 0.1\Gamma$, and $\Omega = \Gamma$. Constants and optical quantities are taken as $\epsilon_0 = 8.85 \times 10^{-12}$ F/m, $\hbar = 1.05 \times 10^{-34}$ J · s, $\mathbf{d}_{A0} = \mathbf{d}_{B0} = 1.269 \times 10^{-29}$ C m, atomic density $\mathcal{N}/V = 10^{12}$ m^{-3}, $\lambda = 852$ nm, and $k_0 = 2\pi/\lambda$. A Gaussian beam with waist $\omega_0 = 50\lambda$ and parameter $q = 0.1 \times 10^{-6}$ m is assumed, and the dielectric constants are $\epsilon_1 = \epsilon_3 = 2.22$ and $\epsilon_2 = 1 + \chi_A(\omega_p)$.

For $\phi = \pi$ and $\theta = 0$ with $\delta = 0$, the coherence vector reduces to

$$\begin{pmatrix} \rho_A \\ \rho_B \end{pmatrix} = \frac{8\Omega^2}{[4\Omega^2 - \Delta(2\Delta + i\Gamma)]^2} \times \begin{pmatrix} \Delta - \dfrac{\Delta^2(2\Delta + i\Gamma)}{4\Omega^2} & 0 \\ 0 & \Delta - \dfrac{\Delta^2(2\Delta + i\Gamma)}{4\Omega^2} \end{pmatrix} \begin{pmatrix} \Omega_{A0} \\ \Omega_{B0} \end{pmatrix} \tag{41}$$

In this configuration, the off-diagonal elements vanish identically, meaning that the two probe channels are completely decoupled. The DT system therefore separates into two independent Λ-type subsystems, each behaving as an isolated EIT channel. No coherent mixing occurs between ρ_A and ρ_B, and the optical response of each probe is governed solely by its own transition pathway.

Optics EXPRESS

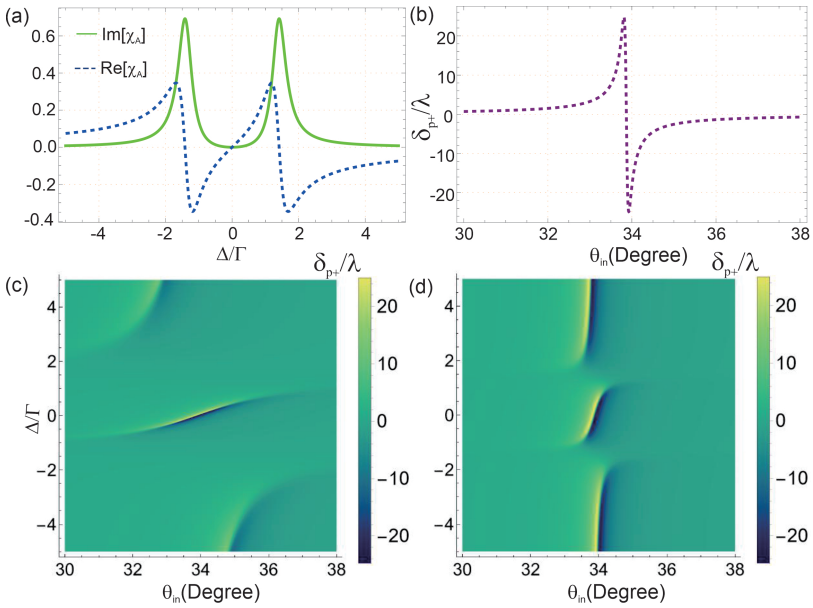


Fig. 6. (a) Dependence of the medium susceptibility on the normalized probe detuning Δ/Γ, where the solid (dashed) trace represents the absorptive (dispersive) component. (b) Transverse photonic spin Hall shift δ_{p+} as a function of the incidence angle θ_{in} for resonant probe detuning $\Delta = 0$ and $\mathcal{N}/V = 10^{12}$ m^{-3}. (c) Density plot of photonic spin Hall shift δ_{p+} as a function of the incidence angle θ and probe detuning Δ/Γ for $\mathcal{N}/V = 10^{12}$ m^{-3}. (d) The same quantity δ_{p+} versus θ_{in} when the number density is decreased by one decade to $\mathcal{N}/V = 10^{11}$ m^{-3}. The calculations assume $\Gamma = 1$ MHz, $\delta = 0$, $\phi = \pi$, $\theta = 0$, probe amplitudes $|\Omega_{A0}| = |\Omega_{B0}| = 0.1\Gamma$, and $\Omega = \Gamma$. Further constants are $\epsilon_0 = 8.85 \times 10^{-12}$ F/m, $\hbar = 1.05 \times 10^{-34}$ J · s, $\mathbf{d}_{A0} = \mathbf{d}_{B0} = 1.269 \times 10^{-29}$ C m, $\lambda = 852$ nm, and $k_0 = 2\pi/\lambda$. A Gaussian beam with waist $\omega_0 = 50\lambda$ and parameter $q = 0.1 \times 10^{-6}$ m is used. The dielectric constants are chosen as $\epsilon_1 = \epsilon_3 = 2.22$ and $\epsilon_2 = 1 + \chi_A(\omega_p)$.

In contrast, for $\phi = 0$ and $\theta = 0$ at $\delta = 0$, the coherence vector becomes

$$\begin{bmatrix}\rho_A\\ \rho_B\end{bmatrix} = \frac{-2}{\Delta(2\Delta + i\Gamma)\left(2 - \frac{\Delta(2\Delta+i\Gamma)}{4\Omega^2}\right)} \times \begin{bmatrix}\Delta - \frac{\Delta^2(2\Delta+i\Gamma)}{4\Omega^2} & -\Delta e^{i\theta_{in}}\\ -\Delta e^{-i\theta} & \Delta - \frac{\Delta^2(2\Delta+i\Gamma)}{4\Omega^2}\end{bmatrix}\begin{bmatrix}\Omega_{A0}\\ \Omega_{B0}\end{bmatrix} \tag{42}$$

Unlike the previous case, the off-diagonal elements are now nonzero, introducing coherent coupling between the two probe fields. The DT system no longer decomposes into independent subsystems; instead, it behaves as a symmetric (degenerate) double-Λ structure with mutual interaction between the channels [19]. This inter-probe coherence fundamentally alters the susceptibility spectrum and, consequently, the PSHE behavior.

Figures 6 and 7 display the optical susceptibility and the associated transverse PSHE shift for zero two-photon detuning ($\delta/\Gamma = 0$) under two phase configurations, $\phi = \pi$ and $\phi = 0$ (with $\theta = 0$). In both cases, the medium exhibits a single EIT transparency window centered at resonance ($\Delta/\Gamma = 0$), where $\mathrm{Im}[\chi_A] \to 0$ and the dispersive component $\mathrm{Re}[\chi_A]$ shows a steep slope. Consequently, the overall PSHE behavior in the two figures is qualitatively similar as seen

Optics EXPRESS

in panel (b) of Figs. 6 and 7: the largest transverse spin-dependent shifts occur in the low-loss region around resonance, confirming that strong dispersion combined with negligible absorption is the key requirement for enhancing PSHE.

The primary distinction between the two phase settings lies in the width of the transparency window. For $\phi = \pi$ (Fig. 6), the EIT feature is relatively narrower, leading to a sharper dispersive variation confined to a smaller detuning interval. As a result, the enhanced PSHE is more localized around resonance and varies more rapidly with detuning. In contrast, for $\phi = 0$ (Fig. 7), the transparency window becomes broader and is bounded by absorption peaks shifted farther from resonance. This broader low-loss region supports a wider detuning range over which significant PSHE can be sustained. Thus, while the general structure of the PSHE maps remains similar in both cases, the detuning span and smoothness of the transverse shift reflect the different transparency bandwidths.

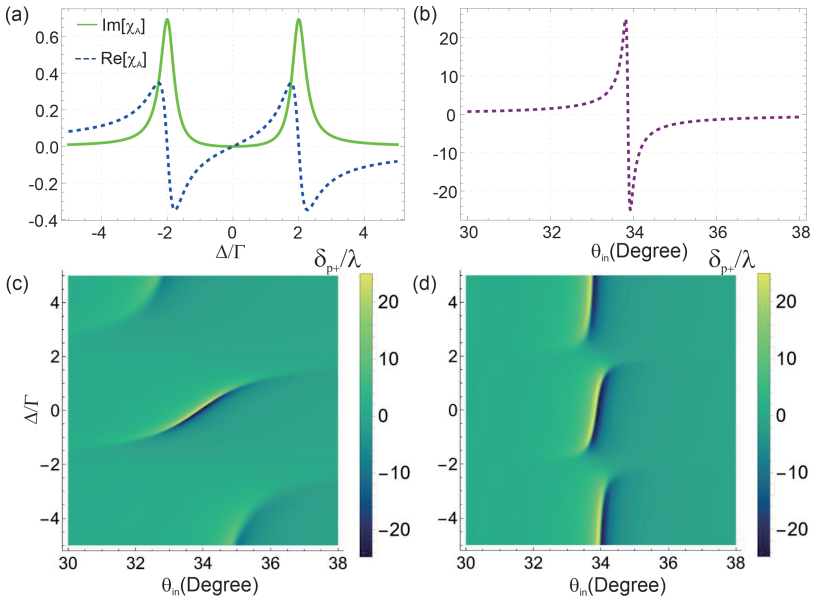


Fig. 7. (a) Absorption (solid curve) and dispersion (dashed curve) of the susceptibility as functions of the scaled probe detuning Δ/Γ. (b) Transverse photonic spin Hall shift δ_{p+} versus incidence angle θ_{in} for $\Delta = 0$ and a number density $\mathcal{N}/V = 10^{12}$ m^{-3}. (c) Density plot of photonic spin Hall shift δ_{p+} versus incidence angle θ_{in} and probe detuning Δ/Γ for a number density $\mathcal{N}/V = 10^{12}$ m^{-3}. (d) The same angular dependence of δ_{p+} when the density is reduced by one decade to $\mathcal{N}/V = 10^{11}$ m^{-3}. The parameter set used is: $\Gamma = 1$ MHz, $\delta = 0$, $\phi = 0$, $\theta = 0$, $|\Omega_{A0}| = |\Omega_{B0}| = 0.1\Gamma$, and $\Omega = \Gamma$, together with $\epsilon_0 = 8.85\times10^{-12}$ F/m, $\hbar = 1.05\times10^{-34}$ J · s, $\mathbf{d}_{A0} = \mathbf{d}_{B0} = 1.269\times10^{-29}$ C m, $\lambda = 852$ nm, and $k_0 = 2\pi/\lambda$. A Gaussian beam is assumed with $\omega_0 = 50\lambda$ and $q = 0.1 \times 10^{-6}$ m. The dielectric constants are taken as $\epsilon_1 = \epsilon_3 = 2.22$ and $\epsilon_2 = 1 + \chi_A(\omega_p)$.

The influence of atomic density follows the same systematic trend for both phase configurations. At higher density ($N/V = 10^{12}$ m^{-3}), the light–matter interaction is stronger, producing steeper dispersion and therefore larger transverse shifts. Reducing the density by one order of magnitude weakens the susceptibility, which directly lowers the magnitude of the PSHE and smoothens its detuning dependence. Importantly, although the amplitude of the shift decreases, its spectral location continues to coincide with the transparency window in both phase settings. Therefore, for $\delta = 0$ the two phase configurations lead to quantitatively different but qualitatively similar PSHE responses. Both exhibit maximal transverse displacement within the EIT window; however,

Optics EXPRESS

$\phi = 0$ yields a broader transparency band and hence a wider operational range for enhanced PSHE, whereas $\phi = \pi$ produces a narrower and more sharply varying response.

5. Concluding remarks

In conclusion, we have shown that the transverse PSHE can be actively engineered in a double-cavity system embedding a double-tripod atomic medium. Through the interplay of quantum interference and cavity-induced transparency, the polarization-dependent transverse shift originates from steep dispersion in low-loss spectral regions and exhibits strong sensitivity to two-photon detuning, the closed-loop control-field phase, and atomic density. Our analysis demonstrates that both the magnitude and sign of the spin-dependent displacement can be continuously tuned, with pronounced enhancement near critical incidence angles. The additional internal degrees of freedom inherent to the double-tripod configuration, compared to conventional single-Λ EIT systems, enable flexible manipulation of the effective refractive index experienced by different spin components. We further derived a propagation-based criterion defining a characteristic medium length for suppressing inter-channel coupling, and verified that this condition is well satisfied under experimentally relevant parameters. These results highlight atom–cavity platforms as versatile systems for reconfigurable spin–orbit photonic control and suggest promising applications in precision beam steering, tunable spin-dependent photonic elements, and weak-measurement-enhanced optical sensing.

A. Criterion for energy transfer suppression and characteristic length estimate

In the main text, we assume that the probe fields with Rabi frequencies Ω_A and Ω_B can be treated locally when evaluating the atomic response. This approximation is valid provided that the redistribution of energy between the two probe channels remains negligible during propagation through the intracavity DT medium. Throughout this Appendix, q denotes the interaction length through the DT medium, consistent with the notation used in the transfer-matrix calculation in Eq. (30). Since the DT medium occupies the intracavity propagation region considered in the present model, q is the relevant propagation distance over which the probe fields interact with the atomic medium between the cavity mirrors M_1 and M_2.

We begin with the Maxwell-Bloch equations for the probe fields. For the continuous-wave fields considered in this work, the temporal derivatives can be neglected over the short propagation length q. This approximation is justified because the fields are quasi-stationary and the propagation time through the intracavity medium is much shorter than the characteristic temporal variation of the system. The propagation equations, therefore, reduce to

$$\frac{d\mathbf{\Omega}_0}{dz} = i\frac{\alpha\Gamma}{2q}\boldsymbol{\rho}_0, \tag{43}$$

where $\mathbf{\Omega}_0$ and $\boldsymbol{\rho}_0$ are the shorthand vectors introduced in Eq. (11), and ρ_A and ρ_B are the steady-state atomic coherences given in Eq. (19). The optical density is defined as

$$\alpha = n\sigma q, \tag{44}$$

where $n = \mathcal{N}/V$ is the atomic number density and σ is the effective optical cross section.

Substituting the steady-state relation $\boldsymbol{\rho}_0 = \mathbf{M}\mathbf{\Omega}_0$ into Eq. (43), we obtain the closed propagation equation

$$\frac{d\mathbf{\Omega}_0}{dz} = \mathbf{K}\mathbf{\Omega}_0, \qquad \mathbf{K} = i\frac{\alpha\Gamma}{2q}\mathbf{M}. \tag{45}$$

The propagation dynamics is governed by the eigenvalues $\lambda_{1,2}$ of $\mathbf{K}$. Negligible redistribution of energy between the two probe channels requires the accumulated eigenmode phase difference

Optics EXPRESS

over the interaction length q to remain much smaller than unity:

$$|\lambda_1 - \lambda_2| q \ll 1. \tag{46}$$

For the 2×2 propagation matrix $\mathbf{K}$, the eigenvalue difference satisfies

$$|\lambda_1 - \lambda_2|^2 = \left|(K_{11} - K_{22})^2 + 4K_{12}K_{21}\right|. \tag{47}$$

Therefore, the negligible-transfer condition becomes

$$\left|(K_{11} - K_{22})^2 + 4K_{12}K_{21}\right| q^2 \ll 1. \tag{48}$$

Using

$$K_{ij} = i\frac{\alpha\Gamma}{2q} M_{ij},$$

Noting that $M_{11} = M_{22}$, Eq. (48) reduces to

$$\alpha^2\Gamma^2 |M_{12}M_{21}| \ll 1, \tag{49}$$

or equivalently,

$$\alpha\Gamma\sqrt{|M_{12}M_{21}|} \ll 1. \tag{50}$$

From Eqs. (22),(23), the product of the off-diagonal matrix elements is

$$M_{12}M_{21} = \frac{(\Delta^2 - \delta^2)^2}{4\Omega^4\Delta^4} \frac{1}{D^2}\Delta^2 \left[\cos^2\left(\frac{\phi}{2}\right) + \frac{\delta^2}{\Delta^2}\sin^2\left(\frac{\phi}{2}\right)\right]. \tag{51}$$

Substituting Eq. (51) into Eq. (50) gives the general criterion for suppressing energy transfer:

$$\alpha\Gamma \frac{|\Delta^2 - \delta^2|}{2\Omega^2} \frac{\sqrt{\Delta^2\cos^2(\phi/2) + \delta^2\sin^2(\phi/2)}}{\left|\left[\Delta - \frac{(\Delta^2-\delta^2)(2\Delta+i\Gamma)}{4\Omega^2}\right]^2 - \Delta^2\cos^2(\phi/2) - \delta^2\sin^2(\phi/2)\right|} \ll 1. \tag{52}$$

We now analyze several limiting cases of the general propagation criterion to identify regimes in which energy transfer between the probe fields can be neglected. Particular attention is paid to distinguishing between the suppression of energy transfer and the complete absence of coupling due to symmetry or dark-state formation. We evaluate the condition (52) for the parameter regimes considered in the main text. For numerical calculations, $q = 1.0 \times 10^{-7}$ m.

For the case $\Delta = \sqrt{2}\Gamma$, $\phi = \pi$, $|\delta| \ll \Omega$, and $\Omega = \Gamma$, as considered in Figs. 3(a) and 3(b), Eq. (52) reduces to

$$4\alpha\frac{|\delta|}{\Gamma} \ll 1, \tag{53}$$

where the optical density is $\alpha = n\sigma q$ with atomic number density $n = \mathcal{N}/V$. This leads to the constraint on the sample length

$$q \ll \frac{\Gamma}{4n\sigma|\delta|}. \tag{54}$$

For a typical optical transition, $\sigma \approx 3\lambda^2/(2\pi)$. Using $\lambda \sim 852\,\text{nm}$ gives $\sigma \sim 3.5 \times 10^{-13}\,\text{m}^2$. Taking $\delta = 0.1\Gamma$, one obtains $q \ll 7.14\,\text{m}$ for $n = 10^{12}\,\text{m}^{-3}$ and $q \ll 71.4\,\text{m}$ for $n = 10^{11}\,\text{m}^{-3}$. The length q used in numerical calculations is therefore many orders of magnitude smaller than the limits and energy transfer between the probe channels is negligible.

Optics EXPRESS

In the case $\Delta = 0$, $\phi = \pi$ corresponding to Figs. 3(c) and 3(d), Eq. (52) simplifies to

$$\alpha\Gamma\frac{|\delta|}{2\Omega^2} \ll 1, \tag{55}$$

assuming $\Omega \sim \Gamma \gg |\delta|$. Using $\alpha = n\sigma q$, this gives

$$q \ll \frac{2\Omega^2}{n\sigma\Gamma|\delta|}. \tag{56}$$

For $\Omega = \Gamma$, $\delta = 0.1\Gamma$ one finds $q \ll 57.14\,\mathrm{m}$ for $n = 10^{12}\,\mathrm{m}^{-3}$ and $q \ll 571.4\,\mathrm{m}$ for $n = 10^{11}\,\mathrm{m}^{-3}$, so $q = 10^{-7}\,\mathrm{m}$ is well within the allowed range.

For $\Delta = 0$, $\phi = 0$, corresponding to Fig. 5(b), the off-diagonal coupling responsible for energy transfer vanishes under the chosen configuration. Equation (52) therefore indicates complete suppression of inter-channel transfer.

For $\Delta = \pm 2\delta$, $\phi = 0$, corresponding to Fig. 5(c), Eq. (52) becomes

$$\alpha\Gamma\frac{|\Delta^2 - \delta^2|}{2\Omega^2}\frac{|\Delta|}{\left|\left(\Delta - \frac{(\Delta^2-\delta^2)(2\Delta+i\Gamma)}{4\Omega^2}\right)^2 - \Delta^2\right|} \ll 1. \tag{57}$$

Substituting $\Delta = 2\delta$ and keeping only leading-order corrections in $|\delta|/\Omega \ll 1$, the condition simplifies to

$$\alpha \ll 1, \tag{58}$$

which gives

$$q \ll \frac{1}{n\sigma}. \tag{59}$$

With $\sigma \sim 3.5 \times 10^{-13}\,\mathrm{m}^2$, this gives $q \ll 2.86\,\mathrm{m}$ for $n = 10^{12}\,\mathrm{m}^{-3}$ and $q \ll 28.6\,\mathrm{m}$ for $n = 10^{11}\,\mathrm{m}^{-3}$, so that for the length used in numerical calculations $q = 10^{-7}\,\mathrm{m}$ the condition is easily satisfied and energy transfer between the probe fields can be neglected

Finally, for $\phi = \pi$, $\Delta = 0$, and $\delta = 0$, corresponding to the parameter configurations considered in Figs. 6 and 7, the off-diagonal coupling responsible for redistribution between the probe channels vanishes. Equation (52) therefore indicates complete suppression of energy transfer.

These estimates demonstrate that the intracavity thickness used throughout the numerical calculations, $q = 0.1 \times 10^{-6}\,\mathrm{m}$, is far below all characteristic upper bounds obtained from the propagation criterion. Therefore, redistribution of energy between the two probe channels during propagation through the DT medium is negligible, validating the local steady-state susceptibility approximation used in the transfer-matrix and photonic spin Hall effect calculations.

Funding. National Natural Science Foundation of China (Grant No. 12265022); Inner Mongolia Natural Science Foundation (Grant No. 2025MS01005); Elite Revitalizing Inner Mongolia Program (Grant No. 2025TGL05).

Acknowledgments. This work was partly supported by the National Natural Science Foundation of China under Grant No. 12265022, the Inner Mongolia Natural Science Foundation under Grant No. 2025MS01005, and the Elite Revitalizing Inner Mongolia Program under Grant No. 2025TGL05.

Disclosures. The authors declare that they have no conflicts of interest.

Data availability. The data that supports the findings of this study are available from the corresponding author upon reasonable request.

References

1. D. F. Walls and G. J. Milburn, *Quantum Optics* (Springer, Berlin, 1994).
2. M. O. Scully and M. S. Zubairy, *Quantum Optics* (Cambridge University Press, Cambridge, 1997).
3. P. Meystre, *Atom Optics* (Springer, New York, 2001).
4. J. R. Anglin and W. Ketterle, "Bose-einstein condensation of atomic gases," Nature **416**(6877), 211–218 (2002).

Optics EXPRESS

5. S. E. Harris, "Electromagnetically induced transparency," Phys. Today **50**(7), 36–42 (1997).
6. M. D. Lukin, "Colloquium: Trapping and manipulating photon states in atomic ensembles," Rev. Mod. Phys. **75**(2), 457–472 (2003).
7. M. Fleischhauer, A. Imamoglu, and J. P. Marangos, "Electromagnetically induced transparency: Optics in coherent media," Rev. Mod. Phys. **77**(2), 633–673 (2005).
8. M. Fleischhauer and M. D. Lukin, "Dark-state polaritons in electromagnetically induced transparency," Phys. Rev. Lett. **84**(22), 5094–5097 (2000).
9. G. Juzeliūnas and H. J. Carmichael, "Systematic formulation of slow polaritons in atomic gases," Phys. Rev. A **65**(2), 021601 (2002).
10. G. Juzeliūnas and P. Öhberg, "Slow light in degenerate fermi gases," Phys. Rev. Lett. **93**(3), 033602 (2004).
11. J. Zhang, G. Hernandez, and Y. Zhu, "Slow light with cavity electromagnetically induced transparency," Opt. Lett. **33**(1), 46 (2008).
12. J. D. Siverns, J. Hannegan, and Q. Quraishi, "Demonstration of slow light in rubidium vapor using single photons from a trapped ion," Sci. Adv. **5**(10), eaav4651 (2019).
13. E. Paspalakis and P. L. Knight, "Electromagnetically induced transparency and controlled group velocity in a multilevel system," Phys. Rev. A **66**(1), 015802 (2002).
14. H. Hamedi, J. Ruseckas, and G. Juzeliūnas, "Electromagnetically induced transparency and nonlinear pulse propagation in a combined tripod and Λ atom-light coupling scheme," J. Phys. B: At., Mol. Opt. Phys. **50**(18), 185401 (2017).
15. H. R. Hamedi, V. Kudriašov, J. Ruseckas, *et al.*, "Azimuthal modulation of electromagnetically induced transparency using structured light," Opt. Express **26**(22), 28249–28262 (2018).
16. M. Abbas, S. H. Asadpour, Ziauddin, *et al.*, "Goos-hänchen shifts in a combined tripod and Λ atom-light coupling scheme," Phys. Rev. A **110**(2), 023730 (2024).
17. M.-J. Lee, J. Ruseckas, C.-Y. Lee, *et al.*, "Experimental demonstration of spinor slow light," Nat. Commun. **5**(1), 5542 (2014).
18. Q.-Q. Bao, X.-H. Zhang, J.-Y. Gao, *et al.*, "Coherent generation and dynamic manipulation of double stationary light pulses in a five-level double-tripod system of cold atoms," Phys. Rev. A **84**(6), 063812 (2011).
19. H. R. Hamedi, V. Kudriašov, M. Mackoit Sinkevicienė, *et al.*, "Coherent phase control of orbital-angular-momentum light-induced torque in a double-tripod atom-light coupling scheme," Phys. Rev. A **112**(6), 063720 (2025).
20. M. Onoda, S. Murakami, and N. Nagaosa, "Hall effect of light," Phys. Rev. Lett. **93**(8), 083901 (2004).
21. K. Y. Bliokh, F. J. Rodríguez-Fortu no, F. Nori, *et al.*, "Spin–orbit interactions of light," Nat. Photonics **9**(12), 796–808 (2015).
22. K. Y. Bliokh and Y. P. Bliokh, "Conservation of angular momentum, transverse shift, and spin hall effect in reflection and refraction of an electromagnetic wave packet," Phys. Rev. Lett. **96**(7), 073903 (2006).
23. J. Sinova, S. O. Valenzuela, J. Wunderlich, *et al.*, "Spin hall effects," Rev. Mod. Phys. **87**(4), 1213–1260 (2015).
24. O. Hosten and P. Kwiat, "Observation of the spin hall effect of light via weak measurements," Science **319**(5864), 787–790 (2008).
25. F. Cardano and L. Marrucci, "Spin–orbit photonics," Nat. Photonics **9**(12), 776–778 (2015).
26. A. Aiello, N. Lindlein, C. Marquardt, *et al.*, "Transverse angular momentum and geometric spin hall effect of light," Phys. Rev. Lett. **103**(10), 100401 (2009).
27. X. Yin, Z. Ye, J. Rho, *et al.*, "Photonic spin hall effect at metasurfaces," Science **339**(6126), 1405–1407 (2013).
28. P. Dong, J. Xu, and J. Cheng, "Enhanced photonic spin hall effect and its sensing application via optical tamm state based on nanocomposites," Phys. Plasmas **31**(1), 012103 (2024).
29. Y. Xiang, X. Jiang, Q. You, *et al.*, "Enhanced spin hall effect of reflected light with guided-wave surface plasmon resonance," Photonics Res. **5**(5), 467–472 (2017).